ELSEVIER

Journal of Chromatography A, 827 (1998) 259–267

JOURNAL OF CHROMATOGRAPHY A

Application of the two-film theory to the determination of mass transfer coefficients for bovine serum albumin on anion-exchange columns

Ernst Hansen, Jørgen Mollerup*

Engineering Research Centre IVC-SEP, Department of Chemical Engineering, Technical University of Denmark, DTU, Building 229, 2800 Lyngby, Denmark

Abstract

The paper describes a method of simultaneous determination of the external and the solid-phase mass-transfer coefficients from frontal analysis data. The protein flux to the solid particles is determined from the slope of the breakthrough curve and the mass-transfer coefficients are determined by fitting the two-film model to the experimentally determined flux. The two-film model is compared with two apparent overall driving force models: the apparent overall mobile phase driving force model and the apparent overall solid-phase driving force model. The experiments show that the apparent overall driving force models fail to describe the flux correctly and this is substantiated by the theory. Results obtained with bovine serum albumin on the anion-exchange media Q HyperD, Source, and Poros show that the external film resistance is significant for Reynolds numbers less than one. The experimental Sherwood numbers are lower than expected and their dependence on the Reynolds number are much higher than expected.

Keywords: Mass transfer; Adsorption isotherms; Albumin

1. Introduction

For large molecules such as proteins the dispersion in an ion-exchange chromatographic column is caused mainly by the mass-transfer resistance. The resistance can be divided into an external film resistance covering the transfer from the mobile phase to the particle surface and a particle resistance covering the transfer from the interphase to the adsorbing phase. The particle resistance includes either pore diffusion, solid (surface) diffusion or both (parallel diffusion). The mass transfer can in most cases be described by the linear driving force approximation. Although a more correct description for the solid-phase mass transfer is obtained using a diffusion term, the linear driving force approximation is adequate in most cases. For solid diffusion Yoshida et al. [1] showed that the approximation is satisfactory when the scaled mass-transfer resistance ratio (solid over external) is less than 5.

A simple approach is the use of an apparent overall driving force model in which the mass flux is calculable as an overall linear driving force multiplied by an overall mass-transfer coefficient. This approach is, however, only applicable when the isotherm is linear or when pore diffusion controls. The apparent overall driving force model is often thought of as a one parameter model. However, the overall mass-transfer coefficient is a lumped parameter comprising the velocity dependent external film resistance, the solid-phase resistance, and in the case

*Corresponding author. Tel.: +45 4525 2866; fax: +45 4588 2258; e-mail: jm@kt.dtu.dk

0021-9673/98/$ – see front matter
PII: S0021-9673(98)00791-2

of solid diffusion, the equilibrium ratio which depends on the salt concentration and the pH in the mobile phase. The resistances are only additive if the equilibrium ratio is independent of the solute concentration, as it is for linear isotherms.

When the isotherm is non-linear and solid diffusion dominates over pore diffusion an overall mass-transfer coefficient is of cause still calculable. Unfortunately, owing to the non-linear isotherm, it becomes a function of the interfacial and the bulk compositions of the solute, therefore it is no longer convenient to use the concept of overall mass-transfer coefficients [2]. In the case of non-linear mass-transfer, the flux equation must be solved simultaneously with the algebraic expression for the equilibrium relation to determine the interfacial composition [3]. The model parameters are, a velocity dependent external film resistance, a constant solid-phase resistance and the isotherm. This subject will be addressed in the paper.

To model parallel diffusion in the solid particle requires a knowledge of the diffusion coefficients in the pore phase and in the solid-phase as well. It has been investigated by Yoshida et al. [4] in cases where the external film resistance can be neglected. We have investigated this model but our data do not permit to discriminate between his approach and our approach where the particle resistance is modelled by a single resistance.

2. Theory

In this work we use the single porosity model where the particles are considered a single homogenous phase. The flux is described by film models using the linear driving force approximation.

2.1. Apparent overall driving force models

Two distinct apparent overall driving force models for the system are considered, the apparent overall mobile phase driving force model and the apparent overall solid-phase driving force model. The corresponding flux equations are:

Apparent overall mobile phase driving force model

$$\frac{\partial q}{\partial t} = \frac{6}{d_p} \cdot K_c(c - c^*) \tag{1}$$

Apparent overall solid-phase driving force model

$$\frac{\partial q}{\partial t} = \frac{6}{d_p} \cdot K_q(q^* - q) \tag{2}$$

where c^* is a hypothetical mobile phase concentration in equilibrium with q, and q^* is a hypothetical solid-phase concentration in equilibrium with c, K_c and K_q are the respective apparent overall mass-transfer coefficients, and $6/d_p$ is the surface to volume ratio for spherical particles. The apparent overall driving forces are $(c-c^*)$ and (q^*-q), respectively.

2.2. Two-film model

In the two-film theory the linear driving forces are $(c-c_0)$ and (q_0-q) where subscript 0 denotes a concentration at the interface of the two-films at which c_0 and q_0 per definition are in equilibrium, that is

$$\frac{\partial q}{\partial t} = \frac{6}{d_p} \cdot k_f(c - c_0) = \frac{6}{d_p} \cdot k_s(q_0 - q) \tag{3}$$

In this work k_f is a velocity dependent external mass-transfer coefficient and k_s is the solid-phase mass-transfer coefficient. $1/k_f$ and $1/k_s$ are denoted the external and solid-phase resistances.

2.3. Constant pattern solutions

2.3.1. The apparent overall driving force models

The Langmuir isotherm often describes the adsorption of a single protein on an ion-exchange medium quite well, therefore it is used in this work. The hypothetical equilibrium concentrations in the apparent overall driving force models, Eqs. (1) and (2), are calculable as

$$q^* = \frac{q_{max} bc}{1 + bc} \text{ and } c^* = \frac{q}{b(q_{max} - q)} \tag{4}$$

where q_{max} is the maximum capacity.

At constant pattern the mobile and solid-phase concentrations are related by [5]

$$\frac{q}{q_F} = \frac{c}{c_F} \tag{5}$$

where c_F is the feed concentration and q_F the corresponding equilibrium concentration. For constant pattern the flux equations become ordinary differential equations. It is convenient to introduce the dimensionless concentrations $x = c/c_F$ and $y = q/q_F$, therefore the constant pattern relation, Eq. (5), becomes $y = x$. Inserting the Eqs. (4) and (5) in the Eqs. (1) and (2), the flux can be expressed as a function of x

$$\frac{dq}{dt} = q_F \cdot \frac{dx}{dt} = \frac{6}{d_p} \cdot K_c c_F \cdot \frac{\beta x(1-x)}{1+\beta(1-x)} \tag{6}$$

and

$$\frac{dq}{dt} = q_F \cdot \frac{dx}{dt} = \frac{6}{d_p} \cdot K_q q_F \cdot \frac{\beta x(1-x)}{1+\beta x} \tag{7}$$

where $\beta = bc_F$.

2.3.2. Two-film model

Inserting the Langmuir expression and the constant pattern relation in the two-film model, Eq. (3), yields

$$\delta(x - x_0) = \frac{(1+\beta)x_0}{1+\beta x_0} - x \tag{8}$$

where δ is the scaled mass-transfer resistance ratio

$$\delta = \frac{k_f c_F}{k_s q_F} \tag{9}$$

The dimensionless interfacial mobile phase concentration x_0 is obtained by solving Eq. (8), which in the present case can be solved analytically. The flux in the two-film model is expressed as a function of x by solving Eq. (8) for x_0 and inserting in Eq. (3). The solution is

$$\frac{dq}{dt} = q_F \cdot \frac{dx}{dt} = \frac{6}{d_p} \cdot k_f c_F (x - x_0) \tag{10}$$

where

$$x_0 = D(x) + \sqrt{[D(x)]^2 + \frac{x(1+\delta)}{\delta\beta}} \tag{11}$$

with

$$D(x) = \frac{1}{2} \cdot \left(x + \frac{x}{\delta} - \frac{1}{\beta} - \frac{1}{\delta} - \frac{1}{\delta\beta} \right) \tag{12}$$

2.4. The breakthrough curves

The breakthrough curves, $x(t)$, are obtained by integrating the flux expressions. The apparent overall driving force models, the Eqs. (6) and (7), have analytical solutions while the two-film model does not. The main difference between the apparent overall driving force model and the two-film model is that where as the driving force in the apparent overall driving force models depends on the isotherm parameters and feed concentration alone, the driving force in the two-film model depends also on the scaled mass-transfer resistance ratio δ because x_0 depends on δ.

The inflection point on the breakthrough curves corresponds to the maximum of the flux curves. The stationary points of the three models, Eqs. (6), (7), (10) are

The apparent overall mobile phase driving force model

$$x'' = \frac{1+\beta-\sqrt{1+\beta}}{\beta} \tag{13}$$

The apparent overall solid-phase driving force model

$$x'' = \frac{\sqrt{1+\beta}-1}{\beta} \tag{14}$$

The two-film model

$$x'' = \frac{1}{1+\delta} \cdot \left(1 + \frac{(\delta-1)(\sqrt{1+\beta}-1)}{\beta} \right) \tag{15}$$

where x'' is the value of x at the inflection point corresponding to a maximum of the flux. The inflection point in the two-film model depends on the scaled mass-transfer resistance ratio δ and $\beta = bc_F$, whereas it in the apparent overall driving force models depends on β only. When δ in Eq. (15) approaches 0, that is when $\delta < 0.1$, it indicates that the flux is controlled by the external film resistance therefore Eq. (15) reduces to Eq. (13). On the other hand, when δ becomes large, $\delta > 10$, the solid-phase resistance is controlling and Eq. (15) reduces to Eq. (14). The two-film model thus coincide with the

apparent overall driving force models when a single resistance controls.

3. Experimental

3.1. Chemicals

Bovine serum albumin, BSA (A6918) and Bis–Tris buffer (B-9754) were from Sigma (St. Louis, MO, USA) both with a purity of 98% according to the manufacturer. NaCl (1.06404.1) was from Merck (Darmstadt, Germany) and 5 *M* HCl (Lab00440) and 5 *M* NaOH (Lab00334) were from Bie & Berntsen, Denmark. Standard solutions for the pH meter calibration were from Radiometer (Copenhagen, Denmark).

3.2. Equipment

A BioCAD Chromatographic Workstation was from Perseptive Biosystems (Cambridge, MA, USA), Milton Roy Spectronic 3000 spectrophotometer and a pH meter (pHM 92) were from Radiometer and 0.45-μm HV filters were from Millipore. The following prepacked columns were used: Resource 15Q (No. 531030) from Pharmacia Biotech (30×6.4 mm), Poros HQ/M (No. 305) from Perseptive Biosystems (100×4.6 mm) and Q HyperD 20 (lot No. 5155) and Q HyperD 35 (lot No. 5266) from BioSepra (100×4.6 mm). A Source 30Q (lot No. 230 230) from Pharmacia Biotech (100×4.6 mm) was packed at Novo Nordisk.

3.3. Procedures

The buffer solutions were prepared by dissolving 25 m*M* Bis–Tris and titrating with HCl to pH 6. Parent solutions were prepared by adding 3 g BSA/l to the buffer and the desired sample solutions were prepared by mixing parent and buffer solutions. Solutions for the non-binding conditions were prepared by adding 0.5 *M* NaCl to the buffer solution. The pH meter was calibrated with standard solutions at pH 4.01 and 7.00. All solutions were filtered through 0.45-μm filters. The concentration in the feed solutions was determined on the Milton Roy spectrophotometer at 280 nm. The breakthrough curves were detected at 280 and 254 nm.

3.4. Experimental measurements

The column was equilibrated with 20 CVs (column volumes) buffer and 40 ml of sample solution was pumped through the system while bypassing the column. The 40 ml was enough to ensure a plateau in the UV signal and the UV detector was zeroed. The sample solution was then passed through the column and the data collection started. The solution was passed through the column well after the breakthrough until a close to constant signal was reached. The column was then bypassed with 5 ml sample solution. The resulting experimental curve is a UV window which starts at zero, passes through a negative plateau and ends with the breakthrough followed by a near constant plateau and finally a step-up to zero from the second bypass. The procedure of bypassing has two purposes: it ensures a step injection originating close to the column and it provides a signal at the feed concentration to be compared with the plateau reached after the breakthrough and finally with the signal from the second bypass whereby one can estimate a possible shift in the detector response. The column was regenerated with 20 CVs of 1 *M* NaCl solution followed by 20 CVs buffer solution. The volume of buffer used in the equilibration and regeneration was later reduced to 10 CVs with no change in the column performance. After approximately 5–10 runs the column was cleaned using the procedure of Sajonz et al. [6]: 5 CVs of 1 *M* NaCl, 5 CVs of 1 *M* NaOH, 5 CVs of 1 *M* HCl, and finally 5 CVs of 1 *M* NaCl. All regeneration and cleaning procedures were carried out at a flow-rate of 0.5 CVs/min. The experimental conditions for the various media are shown in Table 1.

3.5. Data reduction procedure

The model parameters can be obtained by fitting the integral of the flux equations Eqs. (6), (7), (10) to the experimental breakthrough curves or by fitting the flux equations to the experimental flux determined from the slopes of the breakthrough curves. We have chosen the latter method in order to avoid

Table 1
Parameters and experimental conditions

	Q HyperD 35	Q HyperD 20	Source 30Q	Source 15Q	Poros HQ/M
d_p (μm)	49 [7]	20	30	15	20
c_F (g/l)	0.5–3	2	0.2–3	0.1–3 2	
u_0 (cm/h)	400–6000	400–1100	400–1100	200–550	400–1100
ϵ	0.5	0.5	0.5	0.5	0.5
q_{max} (g/l particle)	203	119	66	73	60
b (l/g)	50	50	20	20	20
$k_s \cdot 10^5$ (cm/s)	2.9	4.5	5.1	3.6	13
δ	0.07–7.5	0.06–0.2	0.03–1.0	0.04–0.7	0.08–0.3

numerical integration in the fitting procedure. Further, it is our experience that comparing the experimental flux to the model is a more sensitive way of evaluating the model than comparing the breakthrough curves. The experimental flux was determined by fitting the breakthrough curves to flexible functions with analytical derivatives. The results of this method agreed with results obtained by smoothing and numerical differentiation. The models were fitted to the experimental flux data in the range $0.1<x<0.7$ which covers the mass-transfer zone. The maximum capacity, q_{max}, was determined by matching the model retention time at the centre of mass to the experimental retention time. Due to the extreme non-linearity of the isotherms a confident determination of the b parameter is difficult, therefore it was estimated with appropriate values for each medium.

3.6. Constant pattern evaluation

To verify whether a constant pattern profile was reached in the experiments the following procedure was used: for a given flow-rate and feed concentration the width of the breakthrough curve in milliliters was estimated from the output signal. The experiment was then repeated with a gradient input profile over a significantly larger volume than the estimated width of the breakthrough curve. By comparing the profiles obtained from the step input and various gradient inputs a qualitative measure of the deviation from constant pattern can be obtained. If a constant pattern is reached the profiles will be identical; if not, the profile resulting from the step input must be steeper than the profiles resulting from the gradient inputs. The outlined procedure was applied to the Source 30Q column at a feed concentration of 1 g/l and a superficial velocity of 1060 cm/h. The breakthrough curves for the frontal input (bypass procedure) and the most shallow gradient are compared in Fig. 1. The result is quite convincing; constant pattern is definitely achieved. Since the mass-transfer properties of the media investigated do not differ to a great extent, we assume that a constant pattern has been reached in all the experiments.

4. Results and discussion

Fig. 2 shows a sample breakthrough curve for Q HyperD 35, Source 30Q and Poros HQ/M. It is a characteristic for all our experiments that the feed concentration can only be reached after a very long time. The pseudo plateau is reached at approximately

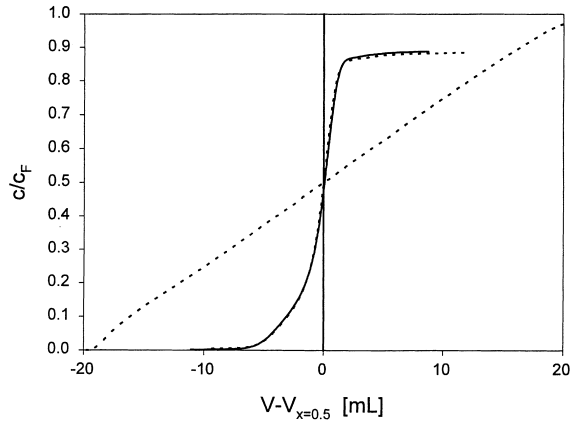

Fig. 1. Breakthrough profiles for Source 30Q at a feed concentration of 1 g/l and a superficial velocity of 1060 cm/h with a step-up input and a 40-ml gradient input.

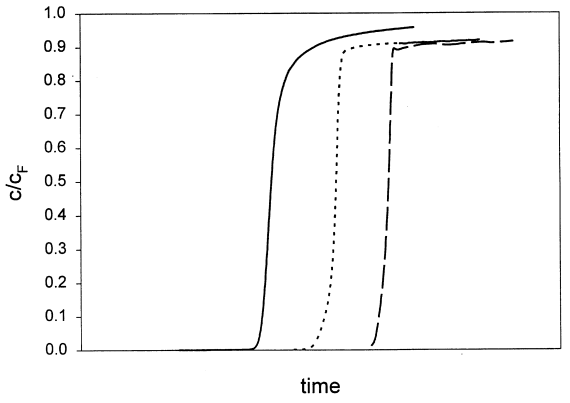

Fig. 2. Breakthrough profiles for Q HyperD 35 (solid line, $c_F=3$ g/l, $u_0=2527$ cm/h), Source 30Q (dotted line, $c_F=2$ g/l, $u_0=1060$ cm/h) and Poros HQ/M (dashed line, $c_F=2$ g/l, $u_0=707$ cm/h).

0.9 c_F for the Source and Poros columns, and at 0.95 c_F for the Q HyperD column.

4.1. Model comparison

The calculated breakthrough curves of the three models for Q HyperD 35 at $c_F=3$ g/l and $u_0=2527$ cm/h are compared with the experimental breakthrough curve in Fig. 3. The results were obtained by integrating the Eqs. (6), (7), (10) using the estimated model parameters. The mass-transfer coefficients in the two-film model, k_f and k_s, were determined by fitting the model to all the experimental flux curves for Q HyperD 35 using a velocity dependent k_f and a constant k_s. The mass-transfer coefficients of the overall driving force models were determined by a fit to the flux data at the conditions shown in Fig. 3. None of the models can of course account for the flattening of the experimental profile observed at high x-values since this phenomenon is not included in any of the models. A plot like Fig. 3 is not a very sensitive way to evaluate the models, since they all seem to give a reasonable description of the steeper part of the breakthrough curve. A more sensitive comparison is to compare the flux profiles. Fig. 4 compares the flux from the experimental breakthrough curve with the three models shown in Fig. 3. The flux is proportional to the slope of the breakthrough curve and its maximum value is at the inflection point of the breakthrough curve, $x=x''$. The location of the inflection point in the apparent overall driving force models is determined by the parameter $\beta=bc_F$ only, see Eqs. (13) and (14), whereas in the two-film model it is greatly influenced by the scaled mass-transfer resistance ratio δ, see Eq. (15). For the data shown in Fig. 4 $\delta=1.9$, indicating that both resistances are important. The two-film model provides a satisfactory fit of the experimental data. The overall models cannot fit the flux data,

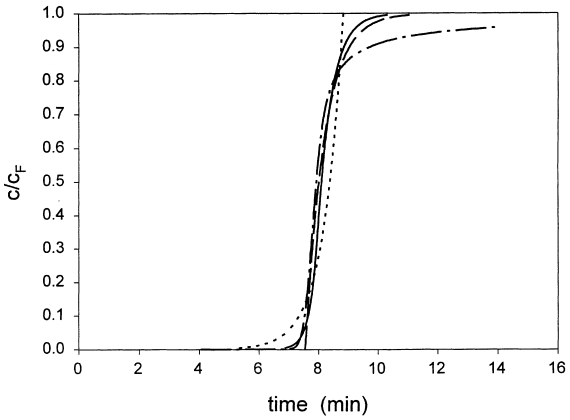

Fig. 3. Comparison of the experimental breakthrough profile for Q HyperD 35 (dash–dotted line, $c_F=3$ g/l, $u_0=2527$ cm/h) and the model profiles for the two-film model (solid line), the apparent overall mobile phase driving force model (dotted line) and the apparent overall solid phase driving force model (dashed line).

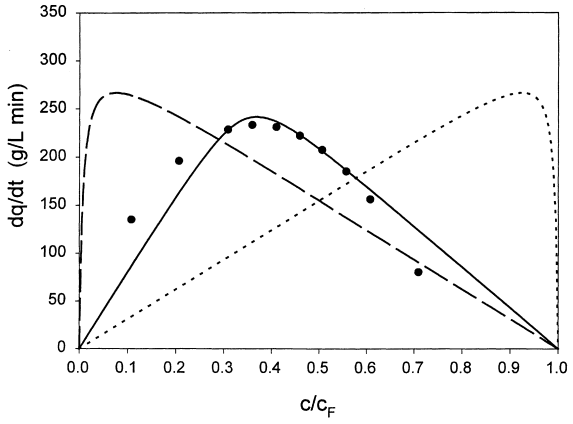

Fig. 4. Comparison of the experimental flux profile for Q HyperD 35 (solid circles, $c_F=3$ g/l, $u_0=2527$ cm/h) and the calculated flux profiles for the two-film model (solid line), the apparent overall mobile phase driving force model (dotted line) and the apparent overall solid phase driving force model (dashed line).

even though the over all mass-transfer coefficients where determined by fitting exclusively to the experimental data as shown in Fig. 4.

When the experimental conditions are varied, either by changing the feed concentration or the velocity, δ changes. Thus the relative importance of the resistances can shift depending on the experimental conditions. The apparent overall driving force models cannot account for this. In general, neither of the overall driving force models can describe the data well when the scaled mass-transfer resistance ratio is in the region $0.1<\delta<10$.

4.2. Comparison with other data

We have measured breakthrough curves for BSA on Resource 15Q under the same experimental conditions as Sajonz et al. [6] and our experimental results are in agreement with theirs. They estimated the apparent overall solid-phase mass-transfer coefficients from the shock layer thickness (SLT). The SLT is the width of the breakthrough curve, usually in time units, between two defined values of x, most often $x=1-\theta$ and $x=\theta$, i.e. $\mathrm{SLT}=t_{(1-\theta)}-t_{\theta}$ where θ is in the range 0.1–0.3. In this way, the model is fitted to match the distance between two points on the breakthrough curve without taking the shape of the breakthrough curve into account. Using this procedure they found an overall mass transfer coefficient proportional to the velocity. We have used their procedure on our experimental results and determined the same values for the parameters.

Fig. 5 compares the experimental flux to the two overall driving force models and the two-film model for Resource 15Q. The overall mass-transfer coefficients were determined from the SLT. The profiles for the overall mobile phase driving force model and the two-film model are almost identical, which indicates that the flux is dominated by the external resistance as can be seen from the values of δ in Table 1 ($\delta\approx0.2$ for Fig. 5). The overall solid-phase driving force model does not describe the flux data well, even though the SLT is the same for the three models.

4.3. Mass-transfer coefficients

Fig. 6 depicts the flux at the inflection point as a function of the superficial velocity for Q HyperD 35, Source 30Q and Poros HQ/M at constant feed concentration. The fluxes show a strong velocity dependence which indicate that the resistance to mass transfer for the three media is strongly dependent on the velocity in the mobile phase. The values for the estimated solid-phase mass-transfer coefficients, the isotherm parameters, and the range of the scaled mass-transfer resistance ratio δ are shown in Table 1. Fernandez et al. [7] determined a k_s value of $1.9\cdot10^{-5}$ cm/s for Q HyperD F. Fig. 7 shows the

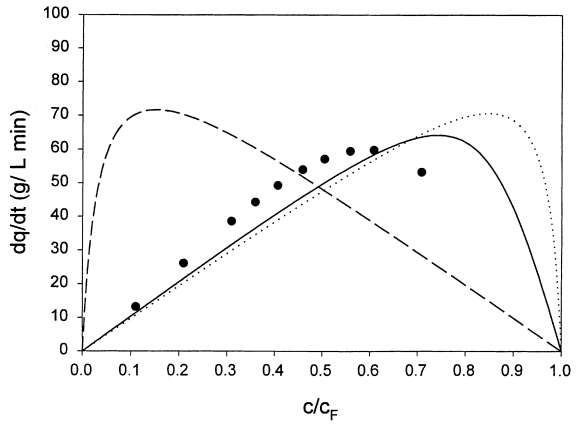

Fig. 5. Comparison of the experimental flux profile for Resource 15Q (solid circles, $c_F=1.5$ g/l, $u_0=187$ cm/h) and the calculated flux profiles for the two-film model (solid line), the apparent overall mobile phase driving force model (dotted line) and the apparent overall solid phase driving force model (dashed line).

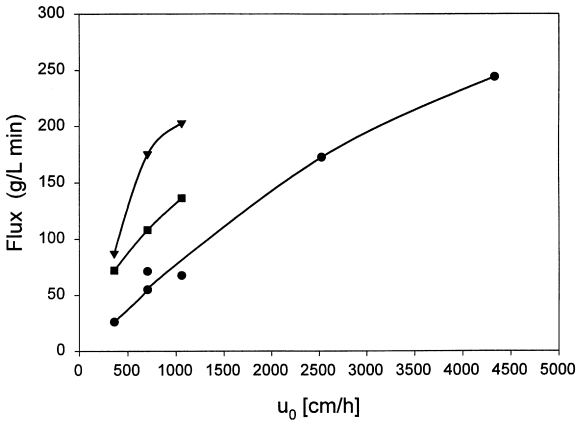

Fig. 6. Experimentally determined velocity dependence of the flux at the inflection point of the breakthrough profile ($c_F=2$ g/l) for Q HyperD 35 (●), Source 30Q (▲) and Poros HQ/M (■).

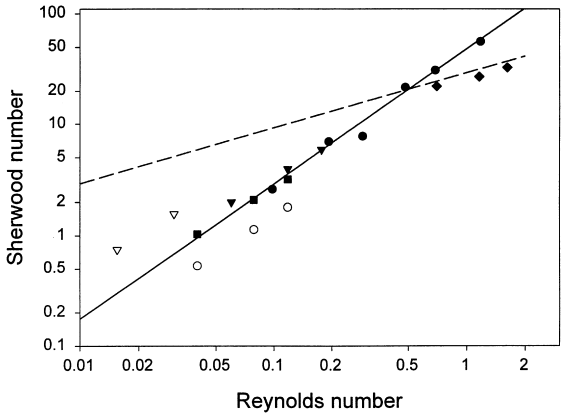

Fig. 7. Sherwood numbers for Q HyperD 35 (●), Q HyperD 20 (○), Source 30Q (▲), Source 15Q (△), Poros HQ/M (■), and data by Fernandez et al. [7] (◇). The solid line represents a correlation of the experimentally determined data by Eq. (16) and the dashed line is the correlation of Carberry [8].

Sherwood number for the external mass-transfer coefficient as function of the Reynolds number. All the data exhibit the same velocity dependence, while the data for the Source 15Q and Q HyperD 20 media fall on each side of the full line representing the best fit to the data given by

$$\mathrm{Sh} = 47.5\mathrm{Re}^{1.22} \tag{16}$$

This correlation is compared with the correlation by Carberry [8]

$$\mathrm{Sh} = 1.15\mathrm{Re}^{1/2}\mathrm{Sc}^{1/3} \tag{17}$$

The Reynolds numbers where calculated assuming a bed porosity of $\epsilon = 0.5$ for all columns. The diffusion coefficient of BSA is $6 \cdot 10^{-7}$ cm^2/s [9] corresponding to a Schmidt number of 16 667. This correlation was used by Fernandez et al. [10]. At low Re, our estimated Sherwood numbers are considerably less than predicted by the correlation of Carberry and show a much stronger velocity dependence. Fernandez et al. [10] estimated Sherwood numbers from experimental data for Q HyperD F at three flow-rates and their results are included in Fig. 7. They concluded that the external resistance was significant. For Resource 15Q Sajonz et al. [6] determined an overall mass-transfer coefficient proportional to the velocity at the same Reynolds numbers as applied here.

The Sherwood numbers we have determined do not reach an asymptotic value of 2 when $\mathrm{Re} \rightarrow 0$ corresponding to a film thickness of half the particle diameter [11]. Carberry [8] stated that it is not inconceivable that at very low flow-rates the boundary layer in a packed bed may develop over a distance greater than one particle diameter. He concluded that in this case the film thickness is proportional to the inverse Reynolds number and as a result the film coefficient will be proportional to the velocity.

Since the Sherwood numbers we have determined exhibit an unexpectedly strong dependence on the velocity, it is appropriate to investigate possible sources of errors. In Eqs. (9)–(12) the parameters q_F and k_f only enter as the ratio k_f/q_F, therefore the estimated values of k_f are proportional to the estimated maximum column capacity but the maximum capacity does not influence the estimated values of k_s. The uncertainty in the column capacities is 15–20%, including the uncertainty in the bed porosity, therefore the uncertainty in k_f is 15–20%. This uncertainty, however, is only reflected in the magnitude of the Sherwood numbers and not in the velocity dependence. The isotherms are strongly non-linear, therefore even a large uncertainty of the *b*-parameter in the Langmuir isotherm will not influence the estimated mass-transfer coefficients significantly. Thus, the uncertainties in the data reduction procedure cannot explain the strong velocity dependence of the Sherwood number.

The influence of the flat upper region of the experimental breakthrough profiles on the estimation of the mass-transfer coefficients is difficult to assess. We find it plausible that this phenomenon has some influence on the location of the inflection point, and to a lesser degree also on the steepness of the breakthrough curve. In our parameter estimation we have included data points up to $x = 0.7$. If only data up to 0.5 were included it would in general increase the Sherwood numbers by no more than 10–20%, but still the estimated Sherwood numbers at low Reynolds numbers would be less than a limiting number of 2.

Symbols

b	Langmuir parameter, (l/g)
c	Mobile phase concentration, (g/l)
c_0	Mobile phase concentration at the interphase, (g/l)
c_F	Feed concentration, (g/l)
CV	Column volume,
d_p	Particle diameter, (μm)
D	Diffusion coefficient, (cm^2/s)
k_f	External film mass-transfer coefficient, (cm/s)
k_s	Solid-phase film mass-transfer coefficient, (cm/s)
q	Solid-phase concentration, (g/l particle)
q_0	solid-phase concentration at the interface, (g/l particle)
q_F	Equilibrium feed concentration in particle, g/l particle
q_{max}	Maximum equilibrium capacity, g/l particle
Re	Reynolds number, $ud_p\rho/\mu$
Sc	Scmidth number, $\mu/\rho D$
Sh	Sherwood number, $k_f d_p/D$
u	Interstitial velocity, cm/s
u_0	Superficial velocity, cm/h
x	Reduced mobile phase concentration, c/c_F
x_0	Reduced concentration at the interphase, c_0/c_F
y	Reduced solid-phase concentration, q/q_F

Greek letters

β	parameter, bc_F
δ	Scaled mass-transfer resistance ratio, $k_f c_F/k_s q_F$
ϵ	Bed porosity,
μ	Viscosity, g/cm s
ρ	Mobile phase density, g/cm^3

Acknowledgements

The authors wish to thank Pharmacia Biotech for supplying the Resource 15Q column and Novo Nordisk for their support.

References

[1] H. Yoshida, T. Kataoka, D.M. Ruthven, Chem. Eng. Sci. 39(10) (1984) 1489.
[2] J. Mollerup, E. Hansen, J. Chromatogr. A 827 (1998) 235.
[3] R.E. Treyball, Mass-Transfer Operations, Ch. 5, McGraw-Hill, New York, 1955.
[4] H. Yoshida, M. Yoshikawa, T. Kataoka, AIChE J. 40(12) (1994) 2034.
[5] P.C. Wankat, Rate Controlled Separations, Ch. 8, Chapman & Hall, 1994, Ch. 8.
[6] P. Sajonz, H. Guan-Sajonz, G. Zhong, G. Guiochon, Biotechnol. Progr. 13 (1997) 170.
[7] M.A. Fernandez, G. Carta, J. Chromatogr. A 746 (1996) 169.
[8] J.J. Carberry, AIChE J. 6 (1960) 460.
[9] M.E. Young, P.A. Carroad, R.L. Bell, Biotechnol. Bioeng. 12 (1980) 947.
[10] M.A. Fernandez, W.S. Laughinghouse, G. Carta, J. Chromatogr. A 746 (1996) 185.
[11] W.L. McCabe, J.C. Smith, P. Harriot, Unit Operations of Chemical Engineering, McGraw-Hill, 5th edition, Singapore, 1993, Ch. 21.